Scaling Laws for Transition from Varicose to Whipping Instabilities in Electrohydrodynamic Jetting

H.H. Xia, A. Ismail, J. Yao and J.P.W Stark

School of Engineering and Materials Science, Queen Mary University of London, London E1 4NS, United Kingdom

Whether an electrified jet breaks up whilst the jet maintains a straight line (varicose), or alternatively the jet trajectory becomes chaotic (whipping), depends on the competition of the interfacial forces. Starting from the competition of normal stresses on the jet surface, we derive scaling laws in different electro-hydrodynamic operating regimes as a function of fluid properties and the flow rate. The onset of whipping occurs when this scaling function reaches a threshold, which is independent of the electric field strength. However, experimental evidence indicates that this onset condition applies only when the viscosity and electrical conductivity of a liquid are small enough. As a result, we further introduce a general parameter to incorporate viscous effects into the scaling law. A unified threshold value for this parameter is found through a substantial number of experiments for liquids having a wide range of properties, and under a wide variety of operational conditions of flow rate.

I. INTRODUCTION

Electrohydrodynamic (EHD) jetting, or also known as electrospray, has been extensively employed including bio-related applications, direct writing, electrospinning, propulsion of microsatellites. These widespread applications are rooted in the evolution of the issued liquid ligament or jet, during which the jet may remain straight (symmetric) or becomes bent (non-symmetric) [1, 2]. When forces induced by surface charge at the interface are trivial compared to the capillary forces [3], the jet is typically straight and breaks up owing to the capillary instability. This mode is known as the varicose (axisymmetric) instability and is the preferred operating mode in many applications especially for EHD printing [4, 5] and electrospray mass spectrometry [6]. The presence of surface charge however provides the possibility that lateral perturbations grow faster than varicose instabilities, and as a result, whipping (or kink) instabilities become dominant. This instability mode is characterized by a curved and stretched jet; this mode is an essential underlying process in electrospinning that can, for example, produce polymer nano-fibers [7, 8].

A number of theoretical models investigating the development of electrified jet instabilities have been developed since the first work contributed by Bassett in the late 19th century [9]. Most of the previous models were derived on the basis of mathematical simplifications of perturbations and specific conditions, such as inviscid or viscous liquids and simplified electric fields [10-13]. More recently, Hartman et al. [14] found that the form of jet breakup depends on the ratio between the normal electric stress and the surface tension stress and above a threshold value the jet starts to whip. Hohman et al. [7] and Fridrikh et al. [8] reported that surface charge density and jet radius play a significant role in the instability mode in electrospinning based on linear stability analysis. Korkut et al. [15] demonstrated that the jet is largely stabilized in ionized surrounding gas, as this can reduce the surface charge density on the jet. López-Herrera and Gañán-Calvo [16] proposed that non-symmetric instabilities dominate when the Weber number is higher than a threshold value, which, however, was not verified. Chen [3] suggested that the surface charge density for the transition of these two modes is an order of magnitude lower than the Rayleigh limit, which is the highest charge density an interface can possess.

Although previous work has provided a basic understanding of jet instabilities, most of the theoretical results contain parameters that are difficult to measure directly in experiments; such parameters are typically the wave number, local electric field, and surface charge density. Due to the lack of a clear connection between parameters that are accessible to direct measurement, such as liquid properties and flow rate, there are few systematic comparisons between experimental and theoretical results. These limitations identify that for applications which are dependent on the jet breakup mode it is particularly valuable to develop a simple, easy-to-use, and robust model (similar to the Reynolds number predicting the laminar and turbulent flow transition) for the prediction of the transition conditions. In this work, we aim to shed further light on the parameters determining EHD jetting instabilities and identify the conditions required to control the instability mode for practical applications. We first start from the competition of the normal forces at the interface, and then introduce the influence of tangential stresses by π-Buckingham theorem. A unified demarcation is finally reached for fluids over a wide range of properties in our experiments and further verified from data in the literature.

II. MATERIALS AND EXPERIMENTAL METHODS

An extensive series of experiments have been conducted to evaluate the conditions required for the transition from varicose to whipping instabilities. Liquids of various properties were used, including 1-Octanol (1-OCT), propylene carbonate (PC), ethylene glycol (EG), ethanol, 1-methoxy-2-propanol (1M2P), triethylene glycol (TEG), and glycerol. The liquids were doped with sodium iodide to adjust the electrical conductivity over a broad range from 0.01 to 490 μS/cm. The details of liquid properties (density ρ, viscosity μ, electrical conductivity K, surface tension γ, and relative permittivity ε_r) are list in Table 1. Experiments with liquid conductivity beyond this range are not considered here. This range in conductivity has been selected because 1) in the case of a liquid with very low electrical conductivity, below this limit, the jet behaves like an uncharged jet, and for which varicose instabilities are always dominant; 2) in the case of a liquid with very high conductivity, the jet becomes so thin that it was not possible to observe clearly the mode of breakup within our experimental configuration.

Table 1 Properties of liquids used in the experiments

Liquid	ρ (kg/m^3)	γ (mN/m)	μ (mPa·s)	ε_r	K (μS/cm)
Ethanol	790	22.3	1.2	24.8	0.76, 5, 10, 14, 24, 50
PC	1207	45.2	2.8	63.0	0.26, 1, 10, 55, 102
1M2P	919	27.0	1.9	12.3	5, 9.3
1-OCT	826	26.1	10.6	10.3	0.64, 8
EG	1110	48.4	21.0	38.7	0.35, 10, 108, 490
TEG	1123	45.3	49.0	23.7	5.5, 9, 25
Glycerol	1262	63.0	1396	42.3	0.01, 1.0, 6, 14

As schematically shown in Fig. 1, the liquid was driven by either gravity or a syringe pump. For the less viscous liquids (including, ethanol, PC, 1M2P, 1-OCT, and some of the experiments with EG), fluid flow was delivered by the gravity head arising from the height difference between the liquid level at the nozzle tip and the fluid surface in a supply reservoir. For the other, higher viscosity liquids, a syringe pump was used due to the high hydraulic resistance in the fluid supply system. For the gravity-driven flow, a nano-flow sensor (Model N-565, Upchurch Scientific) was used to measure directly the feeding flow rate, Q. All the liquids were sprayed using conductive capillary nozzles (New objective, USA) tapered to three different outer diameters, D, at the tips: 30 μm, 150 μm, 310 μm. These nozzles were all treated with hydrophobic liquid crystal material

coating to avoid the liquid wetting back up the nozzle external surface. The extractor electrode had a 2-mm aperture at its center to ensure there was no fluid build-up on this electrode, as this could have distorted the electric field during the completion of an experiment.

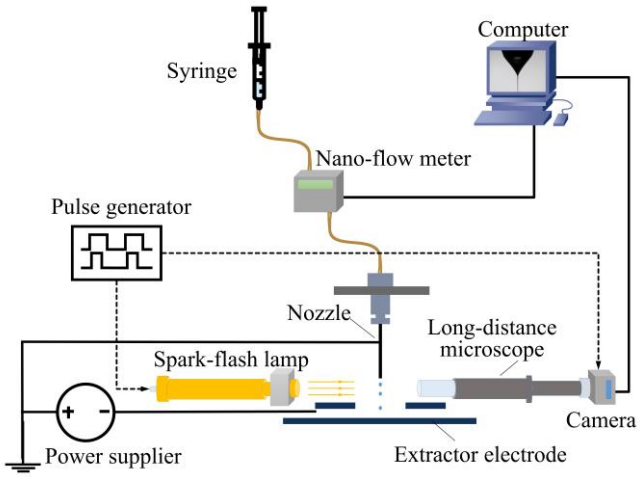

Fig. 1. Schematic of experiment configuration

When a sufficiently high constant negative voltage is applied on the extractor electrode, the electric field transforms the meniscus at the nozzle tip into a conical shape and produces a positively charged jet from the apex of the cone. To identify the influence of the electric potential difference, the electric Bond number is usually used. This dimensionless group is expressed as the ratio between the electric and capillary forces

$$\mathrm{Bo}_{\mathrm{e}} = \frac{\varepsilon_0 E^2 D}{\gamma} , \tag{1}$$

where E is the local electric field strength at the center of the nozzle tip, and ε_0 is the permittivity of ambient air. We estimate the electric field strength using numerical simulations by considering that it resembles the classical value in the configuration where a semi-infinite line is vertical to an infinite plate [17, 18]. The estimated electric field is expressed as $E = 4\sqrt{2}V / \left[D \ln\left(8S / D\right) \right]$, where V is the applied potential difference, and S is the nozzle-electrode spacing (see Appendix A for a detailed fitting). In presenting our experiments we use the electric Bond number, rather than the voltage applied as an independent parameter, together with the dimensionless flow rate to identify experimental conditions.

When the dominant EHD instability is in the whipping mode, the emanated jet usually moves rapidly and is associated particularly with wild off-axis development, leading to difficulty in jet characterization. Some researchers [19, 20] have managed to observe the helical structure of whipping of EHD jetting in liquid surrounding medium, where the characteristic time is dramatically decreased compared to that in ambient air. We have used a different approach and to observe the jet in our experiments a spark-flash lamp with 20 ns illumination duration (High-Speed Photo-Systeme, Germany) was used to ‘freeze’ the jet snapshots. Together with a CCD camera (uEye UI-2230-C, Germany), this fast time-lapse imaging system is capable of capturing images of a jet without blurring. The camera was attached to a long-distance microscopic lens of adjustable magnification; this had a spatial resolution of 1 – 4 pixel/μm.

III. SCALING FOR PREDICTING THE JET INSTABILITY MODE

We consider a Newtonian liquid emanated from a Taylor cone apex into a dielectric medium of very low-viscosity (e.g. air) in the steady cone-jet mode. The impact of surrounding medium on jet instabilities is neglected, since the Reynolds number is always very low for electrospray systems operated in ambient air. In contrast to a nonelectrical jet, an electrified jet undergoes additional electric forces, which allow the dominance of azimuthal modes [7]. As perturbations develop along the jet, the non-uniform distribution of surface charge in the azimuthal direction eventually emerges in a region downstream the jet (see Fig. 2). The resulting electric forces which may bend the jet are divided into normal and tangential components. The normal component originates from the self-repulsion of surface charge, which not only reduces the effective surface tension, but also promotes lateral motion as non-axisymmetric deformation is energetically favorable when electrostatic energy is considered [3, 7]. The role of the tangential stress is complex: on one hand it suppresses the growth of varicose instabilities by accelerating the jet; on the other hand, it may destabilize the jet by generating out-of-phase oscillations between the surface charge and the fluid [7].

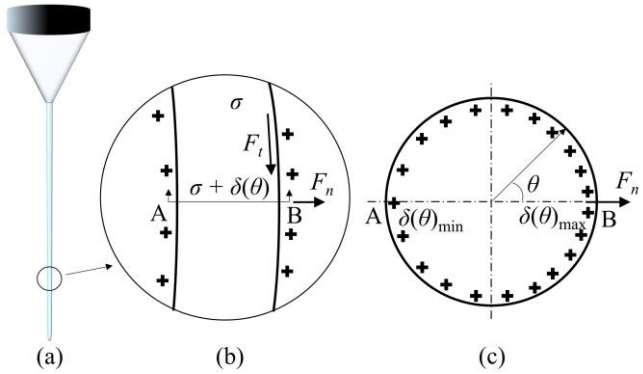

Fig. 2 The schematic of electric forces when surface charge is distributed non-uniformly in the azimuthal (θ) direction: (a) a jet issued from the Taylor cone; (b) electric forces originated from non-axisymmetric perturbations; (c) non-uniform distribution of surface charge of the cross section at AB in (b), where $\delta(\theta)$ denotes small perturbation of surface charge density. F_n is the normal component of the electric force, and F_t is the tangential component.

As also outlined in the introduction, one may determine the instability mode of an electrified jet by examining the competition between the electric forces and capillary forces, which can be expressed as the ratio [3, 8, 14]

$$\Gamma = \frac{\varepsilon_0 E_n^2 R}{\gamma} = \frac{\sigma^2 R}{\varepsilon_0 \gamma}, \tag{2}$$

with *R* being the jet radius. The surface charge density is $\sigma \approx \varepsilon_0 E_n$, where E_n is the normal electric field strength on the interface. The dimensionless parameter Γ can be expressed as a function of fluid properties and operating conditions, if appropriate scaling laws are applied to estimate the dependent parameters, specifically the measured spray current and jet radius [21]. Gañán-Calvo proposed universal scaling laws for the current and jet radius in EHD jetting for six operating regimes [22]. Here, we examine the scaling regimes in our experiments (see Appendix B). Similar to Gañán-Calvo's suggestion, we found our experiments in the "IE", "VE", and "IP" scaling regimes. The most common operating regime is the "IE" regime, where there is "dominance of inertia and electrostatic suction". In this regime, the observed current *I* is mainly due to surface

charge convection, so that $\sigma \approx IR/(2Q)$, where Q is the measured flow rate. Accordingly, the spray current and jet radius are written as

$$I \sim (\gamma K Q)^{1/2}, R \sim \left(\frac{\rho \varepsilon_0 Q^3}{\gamma K} \right)^{1/6}, \tag{3}$$

where K is the liquid electric conductivity, and ρ is density. Substituting these expressions into Eq. (1) yields

$$\Gamma_{\mathrm{IE}} \sim \left(\frac{\rho K Q}{\gamma \varepsilon_0} \right)^{1/2} = (Q/Q_0)^{1/2}. \tag{4}$$

It is interesting to find that in this regime this dimensionless parameter is equal to the square root of the dimensionless flow. This dimensionless flow is defined as the ratio between the feeding flow rate and the commonly defined characteristic minimum flow rate $Q_0 = \gamma \varepsilon_0 / (\rho K)$. In addition to the "IE" regime, the "VE" (dominance of viscous forces and electrostatic suction) regime is typically found for the viscous liquid, glycerol, when the electrical conductivity is so high that the current is mainly attributed to charge convection. Substituting corresponding scaling laws equation (2.21) of Ref. [22] into Eq. (1), we obtain

$$\Gamma_{\mathrm{VE}} \sim \left(\frac{K^2 \mu^3 Q}{\varepsilon_0^2 \gamma^3} \right)^{1/8} = \left(\frac{\mu^3 K}{\rho \varepsilon_0 \gamma^2} \frac{Q}{Q_0} \right)^{1/8}, \tag{5}$$

where μ is the liquid viscosity. Another typical regime is the 'IP' regime, where the inertia and polarization forces are dominant. However, unlike the former regimes, the scaling laws in this regime cannot be applied used in Eq. (2), because the emitted current is not mainly contributed by electric conduction. An interesting finding according to our observations is that the jet instability in this regime was always in the varicose mode. In this regime the liquid electrical conductivity is usually very low or the permittivity is high and as a result the polarization forces are helpful to stabilize the jet. This regime is not considered further in this work, due to the absence of an observable transition between varicose and whipping instability.

The operating diagrams of instability modes of liquids observed for the individual experiments carried with ethanol, PC, EG, and TEG, as a function of Γ vs. $\mathrm{Bo_e}$ are shown in Fig. 3. In all cases at small values of Γ, the jet tends to be in the varicose mode, as denoted by the white shaded region in each plot. The transition from varicose to whipping can clearly be identified for each individual liquid. It can be found that the electric field strength has a minor influence on the transition of jet instability. However, this conclusion seems to be contradictory in previous research. Gomez and Tang [23, 24] claimed that the whipping instabilities become dominant with increased applied potential difference; however, Hartman et al. [14] observed that the transition of the instability mode was independent of the potential difference. It is noted that Gomez used a fluid delivery system where liquids were not controlled by a syringe pump but driven by the pressure difference along the liquid feeding tubes. This total pressure difference increases with the increased applied voltage, due to the increased electric stress versus the capillary pressure at the exit of the emitter. As a result of the increased pressure difference, the flow rate rises [25, 26], and it is therefore this change in flow rate, according to our new results, that is essentially responsible for the change in jet breakup mechanism. In Hartman's experiments, the flow rate was fed and controlled by a

syringe pump, thus independent of the applied voltage. The difference in the liquid feeding system may explain the contrary conclusions by Gomez and Hartman.

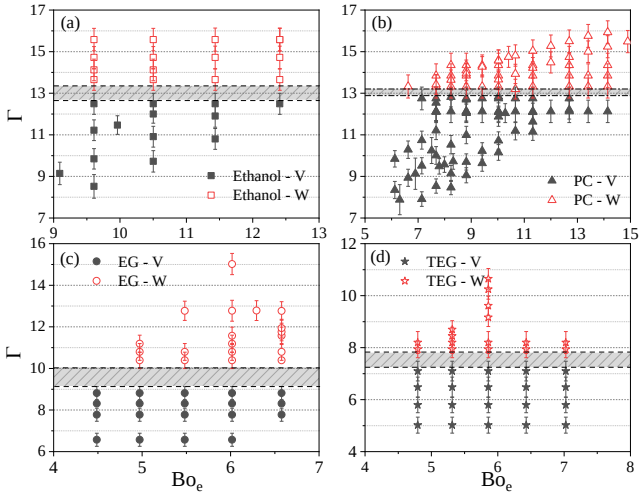

Fig. 3 Operating diagram of the instability mode in the cone-jet electrospray of liquids: (a) ethanol (K = 10 μS/cm), (b) PC (K = 10 μS/cm), (c) EG (K = 10 μS/cm), and (d) TEG (K = 9 μS/cm),. In the legend, V and W denote varicose and whipping, respectively. The error bars stand for uncertainty of measurements of flow rate and fluid properties. The shaded area represents the narrow range over which the transition from varicose to whipping is observed.

In order to confirm this conclusion, we carried out experiments with both syringe controlled flow rate and accurately measured flow rate during hydrostatic pressure style liquid feeding systems. The starting point for these experiments was to initiate the same flow rate (~45 nL/s) in each configuration at the same operating voltage, and then to increase the applied voltage in each case. The liquid used was PC having the same electrical conductivity of 10 μS/cm. Fig. 4 shows the jet breakup remains in the varicose mode at all applied voltages for a constant flow rate, when the liquid (PC) was delivered by the syringe pump. Although the Taylor cone shrank with increasing potential difference, the jet always remained straight, and its length was approximately constant. In contrast, as shown in Fig. 5, the transition from the varicose mode to the whipping mode was observed when varying the potential difference over the same range, for the case where a constant pressure head (height difference) was applied. Although the pressure head was constant, the flow rate increased due to the rise of electric suction force on the Taylor cone under stronger electric fields. With the increasing flow rate, the liquid filament was extended, and the produced droplets started to move away from the axial line. Further increasing the flow rate by increasing the potential difference, the front portion of the jet finally became curved and a spiral structure was observed. We therefore conclude that the transition between the dominant instability modes is insensitive to the applied potential difference for a given liquid, and it is only dependent upon the fluid properties and the flow rate.

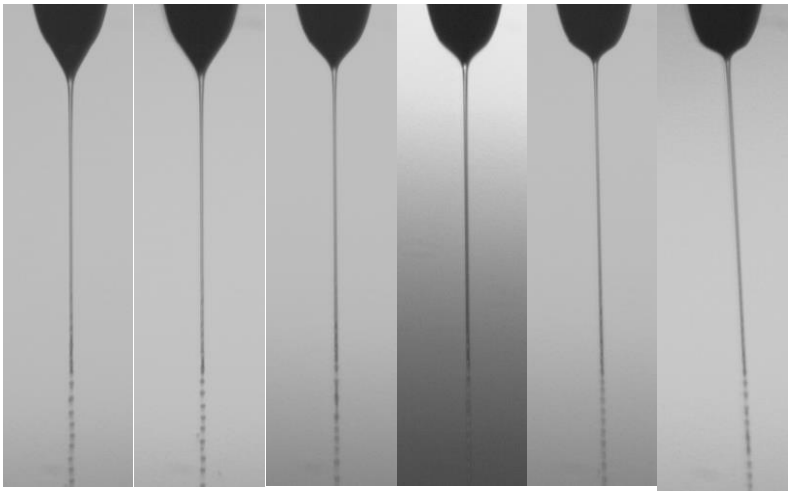

V = 1.40 kV	V = 1.50 kV	V = 1.60 kV	V = 1.70 kV	V = 1.80 kV	V = 1.90 kV
Q = 46 nL/s	Q = 46 nL/s	Q = 46 nL/s	Q = 46 nL/s	Q = 46 nL/s	Q = 46 nL/s

Fig. 4 Jet breakup at various potential differences in the flow-controlled system, where Q = 46 nL/s. The liquid was propylene carbonate (PC) with conductivity of 10 μS/cm. The nozzle outer diameter is 30 μm.

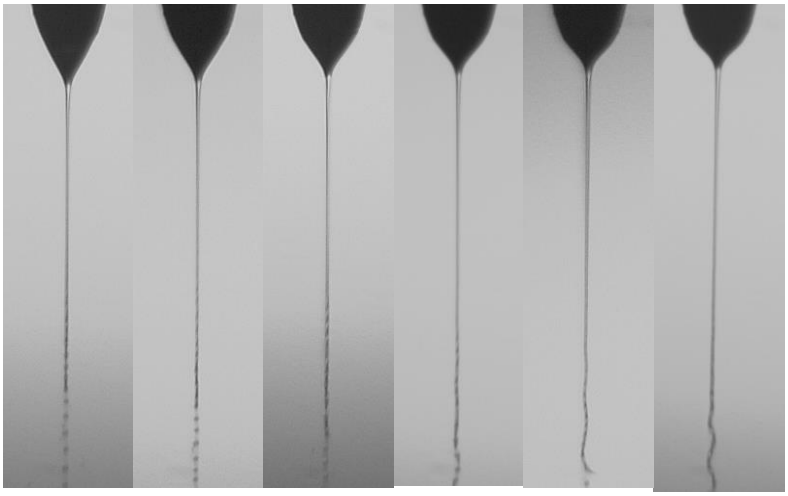

V = 1.40 kV	V = 1.50 kV	V = 1.60 kV	V = 1.70 kV	V = 1.80 kV	V = 1.90 kV
Q = 40 nL/s	Q = 45 nL/s	Q = 50 nL/s	Q = 55 nL/s	Q = 60 nL/s	Q = 66 nL/s

Fig. 5 Jet breakup at various potential differences and the same pressure head for a pressure-controlled system. The liquid was propylene carbonate (PC) with conductivity of 10 μS/cm.

In Fig. 3, the value of Γ at the onset of whipping varies from one liquid to another. The threshold is ~13 for low-viscous liquids, including ethanol and PC. This transition value reduces to ~9.5 and 7.5 for EG and TEG, respectively, indicating a significant influence of viscosity that cannot be ignored. It should be noted that Eq. (4) and (5) are essentially the ratio of the normal stress components on the interface, without considering the competition of the tangential stresses. If there is a tangential electric stress on the interface, there has to be a viscous diffusion term produced as a consequence of interfacial tangential stresses. Although Eq. (5) shows dependence on viscosity, which plays a role in the formation of jet radius, the influence of the viscous term in the local propagation of perturbations is excluded. Increasing viscosity yields higher shear stresses, suppressing the growth of the varicose instability and elongating the jet, which provides the increased possibility for the realization of whipping [7, 13]. The influence of viscosity on the electrified jet dynamics can be described by the dimensionless variable [27-30]

$$\delta_\mu = \left(\frac{\gamma^2 \rho \varepsilon_0}{\mu^3 K} \right)^{1/3}. \quad (6)$$

This variable compares the inertia forces with the viscous forces in electrospray and is only a function of the fluid properties, including the electrical conductivity. When $\delta_\mu < 1$, viscous effects are important. It is interesting to find that δ_μ can be below unity even for the liquids of low viscosity (e.g. ethanol) when the electrical conductivity is increased with dissolved salt. We can now in general form integrate these viscous effects into Eq. (2) to obtain a general empirical function of the two dimensionless groups [29]

$$G = \Gamma^a \delta_\mu^b, \quad (7)$$

where the coefficients *a*, *b* can be determined experimentally and Γ is a function of fluid properties and the flow rate varies in different regimes as specified by Eq. (4) and (5).

As noted previously the majority, but certainly not all cases of electrospray, occur in the so called "IE" regime. Our earlier conclusion, based upon observations, is that the dominant driving mechanism for transition between whipping and varicose break-up of the emitted jet, is dependent upon the flow rate in the system, with negligible dependence upon the electrical Bond number. If we take the value of exponent *a*, to be 2 for simplicity, then the Γ^2 form of *G* captures the flow rate sensitivity of instability mode dependence, being from Eq. (4) simply that $G \propto Q / Q_0$. It is interesting to find similar conclusions reported by Gundabala et al. [18], where the transition from varicose to whipping was observed by increasing the flow rate in a glass-based EHD microfluidics system. Using this value of *a*, in Fig. 6 we plot for all the data the dependence of Γ^2 with respect to δ_μ. In this plot, we identify the electrospray regimes as proposed by Gañán-Calvo for all of our experimental data, together with a grey shaded area when whipping is observed, and no shading when the electrospray is in varicose mode. In each regime we have adopted the relevant definitions of Γ from Eq. (4) through (5). From this plot we note that when $\delta_\mu > 1$, the threshold value of Γ^2, above which whipping instability mode is observed is nearly constant, with a value of ~155. However, when $\delta_\mu < 1$, a different behavior is observed and in this region the influence of the ratio of inertia forces relative to viscous forces becomes apparent, with the influence of viscosity increasing as δ_μ reduces. Indeed, in this region the threshold value for Γ, at the onset of whipping decreases and the viscous impact is increasingly noticeable. It would appear therefore that we can identify two regions: Region I ($\delta_\mu < 1$), wherein a viscous correction is required to capture the threshold transition between instability modes, beyond the simple proportionality of non-dimensional flow rate, which is apparent in Region II, when $\delta_\mu > 1$. For each of the data sets in Region I the appropriate value for Γ, at which the transition between modes is observed, was evaluated and a power law regression was used to identify the dependence of Γ upon δ_μ. The best fit value for $b = -0.33 \pm 0.03$ and accordingly in Region I we can write $G = \Gamma^2 \delta_\mu^{-0.33}$, above which the jet is in the whipping mode. This indicates that the higher viscosity, the more likely the whipping instabilities dominate. In Fig. 7 both our new data and additional datasets from literature [14, 31-33] are also included in a plot of *G* as a function of δ_μ, with the separation between regions highlighted. These additional datasets are consistent with our prediction. It is interesting to find

from Fig. 6 that the onset of whipping occurs most commonly in the IE regime (denoted by the dashed circles) for liquids of not very high viscosity (e.g. $\delta_\mu > 0.01$), where Γ^2 equals the dimensionless flow rate. For highly viscous liquids (e.g. glycerol), electrospinning (whipping) can be likely found when conductivity is sufficiently high to be operated in the VE regime.

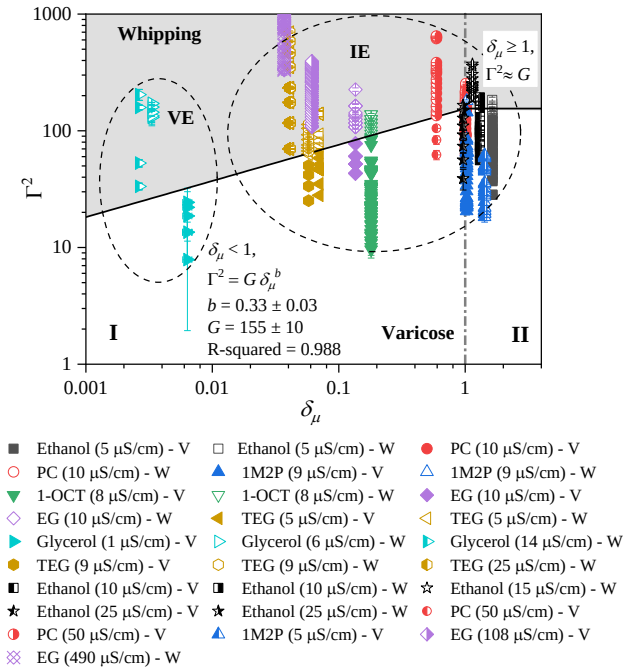

Fig. 6 Operating diagram of instability modes in the cone-jet electrospray in terms of Γ^2 and δ_μ. The criterion for whipping is given by $\Gamma^2 \delta_\mu^{-0.33} > 155$ when $\delta_\mu < 1$, and $\Gamma^2 > 155$, when $\delta_\mu \geq 1$ (grey background). The two dashed circles illustrate the IE and VE regimes, respectively, where different scaling laws were applied.

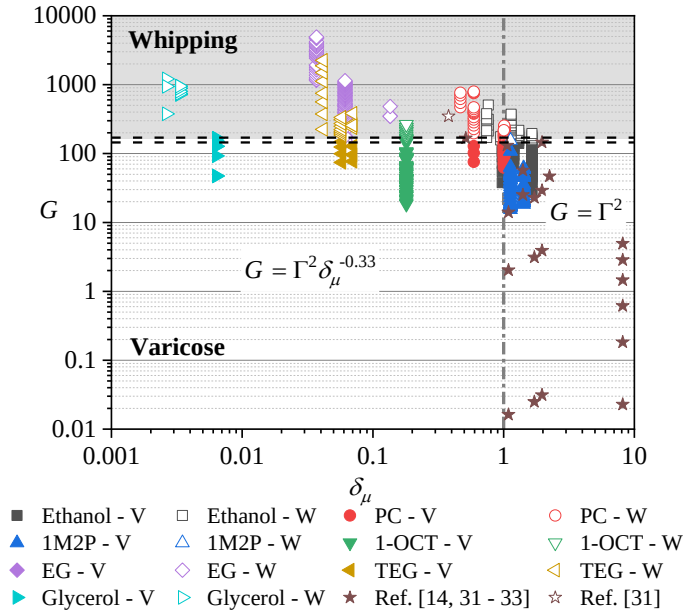

Fig. 7 Demarcation of whipping and varicose modes with the plot of G vs. δ_μ. The two modes are separated by two horizontal dashed lines G = 145 and 165, between which denotes uncertainty of transition from varicose (white) to whipping (grey).

Example images of jet breakup instabilities at typical values of G are shown in Fig. 8. When G < 155, the jet moves along a straight line and breaks up in the varicose mode. When G is slightly above 155, the front portion of the jet starts to bend, showing the transition into the whipping mode. Further increasing G leads to increasingly chaotic/whipping behaviors and producing scattered droplets over a wide range of trajectories. This could be of particular interest in applications of EHD printing where the patterns of printed lines are critical. A line printed using EHD jetting is demonstrated in Fig. 9, the pattern with non-uniform width (sometimes even discontinuity) and the surrounding scattered dots produced in the whipping mode may cause undesirable performance and failure of printed features especially for examples in the applications of printing high-resolution electrical tracks. Such tracks can however be achieved if the jet breaks up in the varicose mode (see Fig. 9 (b)). Indeed, this approach has been demonstrated to achieve line width below 10 μm using nanoparticle inks [34].

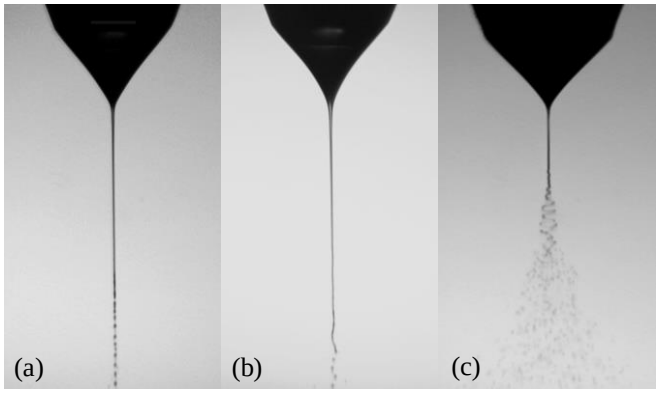

Fig. 8 Examples of the instabilities: (a) varicose mode, G = 36, and (b) transition into the whipping mode, G = 190, (c) whipping mode, G = 800. The working liquid was NaI-doped propylene carbonate. The nozzle tip diameter D = 150 μm.

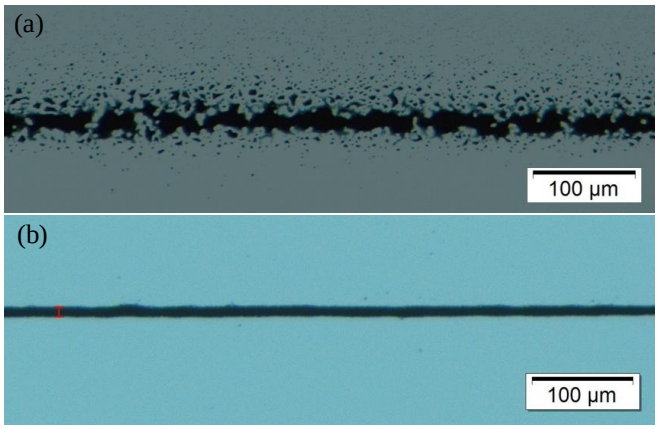

Fig. 9 Printed patterns in (a) the whipping mode and (b) the varicose mode

IV. CONCLUSIONS

This study identifies a dimensionless group *G* that can differentiate between the varicose and whipping instabilities in the stable electrohydrodynamic jetting for liquids of various properties. The form of this parameter varies with operating regimes where different scaling laws for the current and jet radius are applied, and depends on the force competition at the jet interface. When the viscous effect is negligible, the dimensionless form is the ratio of normal stresses at the jet interface and it is observed that there is a constant threshold value found for the mode transition, above which whipping occurs. When viscous effects become more important, including liquids of low viscosity but sufficiently high conductivity, this dimensionless group incorporates the parameter of viscosity in power law dependence. A unified threshold of onset of whipping is found in the viscous and low-viscous regimes. When the parameter exceeds ~155, the non-axisymmetric instabilities dominate, leading to the lateral motion of the jet. With this new formulation, it is now possible to predict the dominant instability mode in an electrospray system as a function of the flow rate for a given liquid.

ACKNOWLEDGMENTS

H. H. X. thanks the China Scholarship Council (CSC) for the financial support. J. Y. acknowledges support from the European Union's Horizon 2020 research and innovation program under grant agreement No.646296. A. S. acknowledges support from the Engineering and Physical Sciences Research Council (UK) under grant No. EP/N509917/1.

APPENDIX

A. Numerical estimation of electric field strength at the nozzle tip

Fig. 10 presents the relationship between the electric field strength at the center of the nozzle tip and the nozzle outer diameter in our experimental configuration. The results were obtained from numerical simulations of electrostatics using the commercial software COMSOL 5.3, where the existence of liquid was not considered.

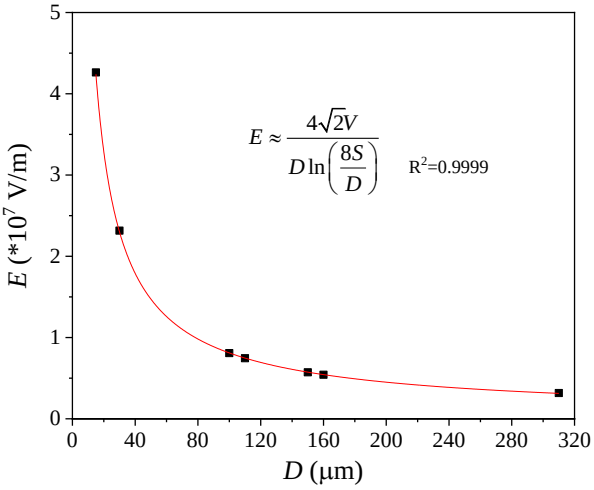

Fig 10. The electric field at the tip of the nozzle as a function of the nozzle diameter according to simulations with COMSOL, where V = 1 kV.

B. Parameter regimes in our experiments

Fig. 11 shows the parameter regimes in our experiments using the same scaling laws in Gañán-Calvo's work [22]. The main regimes are the IE and IP regimes, and the VE regime is only obtained for glycerol of high conductivity. No data in the VP regime was obtained.

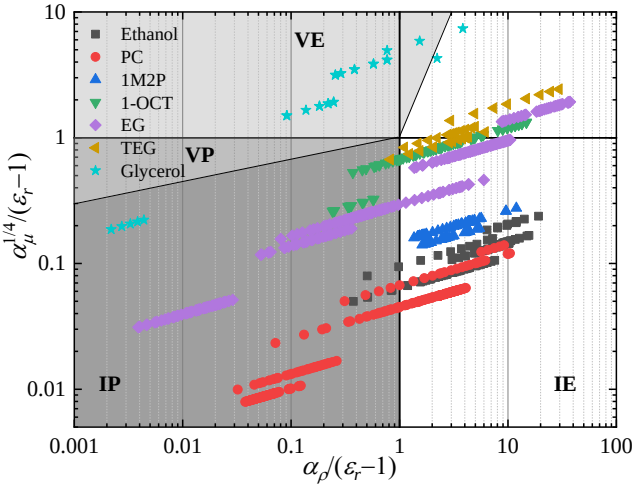

Fig 11. Parameter regimes of the present experiments based on the scaling laws in Ref. [22]: IE (white), IP (dark grey), VP (medium grey) and VE (light grey), where $\alpha_\rho = \rho KQ/(\gamma\varepsilon_0)$, and $\alpha_\mu = K^2\mu^3 Q/(\varepsilon_0^2\gamma^3)$.

References

[1] M. Cloupeau and B. Prunet-Foch, Electrostatic spraying of liquids in cone-jet mode, J. Electrost. 22, 135 (1989).

[2] W. Yang, H. Duan, C. Li, and W. Deng, Crossover of varicose and whipping instabilities in electrified microjets, Phys. Rev. Lett. 112, 054501 (2014).

[3] C. H. Chen, "Electrohydrodynamic stability," in Electrokinetics and Electrohydrodynamics in Microsystems, edited by A. Ramos (Springer, New York, 2011), pp. 177-220.

[4] M. S. Onses, E. Sutanto, P. M. Ferreira, A. G. Alleyne, and J. A. Rogers, Mechanisms, capabilities, and applications of high-resolution electrohydrodynamic jet printing, Small 11, 4327 (2015).

[5] M. D. Paine, M. S. Alexander, K. L. Smith, and J. P. W. Stark, Controlled electrospray pulsation for deposition of femtoliter fluid droplets onto surfaces, J. Aerosol Sci. 38, 315 (2007).

[6] J. B. Fenn, M. Mann, C. K. Meng, S. F. Wong, and C. M. Whitehouse, Electrospray ionization for mass spectrometry of large biomolecules, Science 246, 64 (1989).

[7] M. Hohman, M. Shin, G. Rutledge, and M. Brenner, Electrospinning and electrically forced jets. I. Stability theory, Phys. Fluids 13, 2201 (2001).

[8] S.V. Fridrikh, J. H. Yu, M. P. Brenner, and G. C. Rutledge, Controlling the fiber diameter during electrospinning, Phys. Rev. Lett. 90, 144502 (2003).

[9] A. B. Basset, Waves and jets in a viscous liquid, Am. J. Math. 16, 93 (1894).

[10] G. Taylor, Electrically driven jets, Proc. R. Soc. A 313, 453 (1969).

[11] J. R. Melcher and E. P. Warren, Electrohydrodynamics of a current-carrying semi-insulating jet, J. Fluid Mech. 47, 127 (1971).

[12] A. J. Mestel, Electrohydrodynamic stability of a slightly viscous jet, J. Fluid Mech. 274, 93 (1994).

[13] A. J. Mestel, Electrohydrodynamic stability of a highly viscous jet, J. Fluid Mech. 312, 311 (1996).

[14] R. P. A. Hartman, D. J. Brunner, D. M. A. Camelot, J. C. M. Marijnissen, and B. Scarlett, Jet break-up in electrohydrodynamic atomization in the cone-jet mode, J. Aerosol Sci. 31, 65 (2000).

[15] S. Korkut, D. A. Saville, and I. A. Aksay, Enhanced stability of electrohydrodynamic jets through gas ionization, Phys. Rev. Lett. 100, 034503 (2008).

[16] J. M. López-Herrera and A. M. Gañán-Calvo, A note on charged capillary jet breakup of conducting liquids: experimental validation of a viscous one-dimensional model, J. Fluid Mech. 501, 303 (2004).

[17] L. Loeb, A. Kip, G. Hudson, and W. Bennett, Pulses in negative point-top-plane corona, Phys. Rev. 60, 714 (1941).

[18] V. R. Gundabala, N. Vilanova, and A. Fernández-Nieves, Current-voltage characteristic of electrospray processes in microfluidics, Phys. Rev. Lett. 105, 154503 (2010).

[19] G. Riboux, A. G. Marin, I. G. Loscertales, A. Barrero, Whipping instability characterization of an electrified visco-capillary jet, J. Fluid Mech. 671, 226 (2011).

[20] J. Guerrero, J. Rivero, V. R. Gundabala, M. Perez-Saborid, and A. Fernandez-Nieves, Whipping of electrified liquid jets, Proc. Natl. Acad. Sci. U. S. A. 111, 13763 (2014).

[21] J. Fernández de la Mora, The fluid dynamics of Taylor cones, Annu. Rev. Fluid Mech. 39, 21742 (2007).

[22] A. M. Gañán-Calvo, On the general scaling theory for electrospraying, J. Fluid Mech. 507, 203 (2004).

[23] A. Gomez and K. Tang, Charge and fission of droplets in electrostatic sprays, Phys. Fluids 6, 404 (1994).

[24] K. Tang and A. Gomez, On the structure of an electrostatic spray of monodisperse droplets, Phys. Fluids 6, 2317 (1994).

[25] K. L. Smith, M. S. Alexander and J. P. W. Stark, Voltage effects on the volumetric flow rate in cone-jet mode electrospraying, J. Appl. Phys. 99, 064909 (2006).

[26] K. L. Smith, M. S. Alexander and J. P. W. Stark, The sensitivity of volumetric flow rate to applied voltage in cone-jet mode electrospray and the influence of solution properties and emitter geometry, Phys. Fluids 18, 092104 (2006).

[27] J. F. Rossel-Llompart and J. Fernández de la Mora, Generation of monodisperse droplets 0.3 to 4 μm in diameter from electrified cone-jets of highly conducting and viscous liquids, J. Aerosol Sci. 25, 1093 (1994).

[28] A. M. Gañán-Calvo, J. Dávila and A. Barrero, Current and droplet size in the electrospraying of lliquids. scaling laws, J. Aerosol Sci. 28, 249 (1997).

[29] A. M. Gañán-Calvo, N. Rebollo-Muñoz, J. M. Montanero, The minimum or natural rate of flow and droplet size ejected by Taylor cone-jets: physical symmetries and scaling laws, New J. Phys. 15, 033035 (2013).

[30] A. M. Gañán-Calvo, J. M. López-Herrera, N. Rebollo-Muñoz and J. M. Montanero, The onset of electrospray: the universal scaling laws of the first ejection, Sci. Rep. 6, 32357 (2016).

[31] R. P. A. Hartman, J. P. Borra, D. J. Brunner, J. C. M. Marijnissen, and B. Scarlett, The evolution of electrohydrodynamic sprays produced in the cone-jet mode, a physical model, J. Electrost. 47, 143 (1999).

[32] A. Lee, H. Jin, H. W. Dang, K. H. Choi and K. H. Ahn, Optimization of experimental parameters to determine the jetting regimes in electrohydrodynamic printing, Langmuir 29, 13630 (2013).

[33] I. Park, W. S. Hong, S. B. Kim, and S. S. Kim, Experimental investigations on characteristics of stable water electrospray in air without discharge, Phys. Rev. E 95, 063110 (2017).

[34] A. Said Ismail, J. Yao, H. H. Xia and J. P. W. Stark, Breakup length of electrified liquid jets: scaling laws and applications, Phys. Rev. Appl. 10, 064010 (2018).